Global Change Biology (2008) 14, 1–20, doi: 10.1111/j.1365-2486.2008.01556.x

Evaluating drought effect on MODIS Gross Primary Production (GPP) with an eco-hydrological model in the mountainous forest, East Asia

TAEHEE HWANG*, SINKYU KANG†, JOON KIM‡, YOUNGIL KIM§[1], DOWON LEE§ and LAWRENCE BAND*

*Department of Geography, University of North Carolina at Chapel Hill, Chapel Hill, NC 27599, USA, †Department of Environmental Science, Kangwon National University, Chuncheon, Kangwon-do 200-701, Republic of Korea, ‡Department of Atmospheric Sciences, Yonsei University, Seoul 120-749, Republic of Korea, §Graduate School of Environmental Studies, Seoul National University, Seoul 151-742, Republic of Korea

Abstract

Surface soil moisture dynamics is a key link between climate fluctuation and vegetation dynamics in space and time. In East Asia, precipitation is concentrated in the short monsoon season, which reduces plants water availability in the dry season. Furthermore, most forests are located in mountainous areas because of high demand for agricultural land, which results in increased lateral water flux and uneven distribution of plant available water. These climatic and topographic features of the forests make them more vulnerable to drought conditions. In this study, the eco-hydrological model (Regional Hydro-Ecological Simulation System) is validated with various water and carbon flux measurements in a small catchment in Korea. The model is then extended to the regional scale with fine-resolution remote sensing data to evaluate the Moderate Resolution Imaging Radiometer (MODIS) leaf area index and gross primary productivity (GPP) products. Long-term model runs simulated severe drought effect in 2001 well, which is clearly shown in the ring increment data. However, MODIS GPP does not capture this drought effect in 2001, which might be from a simplified treatment of water stress in the MODIS GPP algorithm. This study shows that the MODIS GPP products can potentially overestimate carbon uptake specifically during drought conditions driven by soil water stress.

Keywords: drought effect, eco-hydrological model, gross primary productivity, MODIS, RHESSys

Received 17 July 2007 and accepted 25 October 2007

Introduction

Recently, eddy covariance measurement has enabled the estimation of turbulent fluxes of heat, water and carbon between vegetation and atmosphere over time scales of hours to years with minimal disturbances (Baldocchi *et al*., 2001; Schimel *et al*., 2002). However, this method typically provides spatially and temporally limited data, restricted to times when atmospheric conditions are steady and to a place of relatively flat terrain where vegetation extends more than 100 times the sampling height (Baldocchi *et al*., 2001). Particularly in mountainous forests like East Asia, where most remaining forests are located in topographically complex mountainous areas unsuitable for agricultural land, its temporal and spatial coverage is much more limited (Schimel *et al*., 2002). In addition, complex topography results in spatially heterogeneous microclimate conditions, redistribution of soil water and increase of water outflow from forest ecosystem, which characterizes temporal and spatial variability of forest carbon flux (Running *et al*., 1987; Band *et al*., 1993; Kang *et al*., 2002, 2006). Surface soil moisture dynamics is a key link between climate fluctuation and vegetation dynamics in space and time (Rodriguez-Iturbe, 2000),

Correspondence: Taehee Hwang, tel. +1 919 923 7537, fax +1 919 962 1537, e-mail: h7666@email.unc.edu

[1]Present address: Department of Geography, McGill University, Montreal H3A 2K6, Canada.

which are not evenly distributed across rugged slopes (Famiglietti & Wood, 1994; Zheng *et al*., 1996; Yeakley *et al*., 1998). Therefore, incorporating lateral hydrological processes and topoclimate patterns into ecosystem processes is crucial to understand the spatial pattern of carbon fluxes in these environments.

Flux measurements are usually constrained by relatively small spatial and temporal scales (Baldocchi *et al*., 2001; Falge *et al*., 2002), whereas global flux estimates are represented by their large spatial and temporal scales. The US National Aeronautics and Space Administration (NASA) Earth Observing System (EOS; http://modis.gsfc.nasa.gov/) currently produces a regular global estimate of gross primary production (GPP) and net primary production (NPP) of the entire terrestrial earth surface at 1 km spatial resolution with algorithms (MOD17A3) designed for the Moderate Resolution Imaging Spectroradiometer (MODIS) sensor aboard the Terra and Aqua platforms (Running *et al*., 2000, 2004; Heinsch *et al*., 2003; Zhao *et al*., 2005). MODIS products require validation to be useful for scientific purposes. However, validation of MODIS products with flux tower information raises important scaling issues. Bridging the gap between these two scales is a major challenge in upscaling flux measurements (Kim *et al*., 2006a). The combination of field measurements, remote sensing and process-based ecological modeling can be a useful tool to bridge these spatio-temporal gaps (Turner *et al*., 2003, 2005). Several flux tower sites have reported clear differences in the pattern of net ecosystem exchange (NEE) depending on temporal and spatial variability of footprints of turbulent flux measurements (Aber *et al*., 1996; Cienciala *et al*., 1998; Kim *et al*., 2006a). Therefore, it is also important to integrate the spatial information of land cover type and vegetation patterns when upscaling flux measurements to regional or global scale.

In this study, a GIS-based, eco-hydrological model [Regional Hydro-Ecological Simulation System (RHESSys)] (Band *et al*., 1993; Tague & Band, 2004) was used as a scaling tool from a small deciduous broadleaf forest (DBF) catchment to a regional watershed scale. The primary advantage of this model is to use streamflow data from a catchment outlet to match the mass balance of water cycle, not affected by topographic and atmospheric conditions. RHESSys considers the spatial variances of microclimate and soil water in simulating water and carbon dynamics of forest ecosystem. Therefore, the model estimates the spatial variances of soil water and fluxes of water and carbon at a regional scale, which would be more effective especially in complex terrain. Daily streamflow data and seasonal leaf area index (LAI) values were used to calibrate the model with both water and carbon cycles. Other field measurements and flux measurements for at least 1 year were used to evaluate model results. After this stepwise calibration strategy at a small catchment scale, the model was simulated to a regional scale by employing spatial vegetation information derived from high-resolution satellite images from the Landsat Enhanced Thematic Mapper plus (ETM+). Finally, regional scale model results were applied to evaluate MODIS land products (LAI and GPP/NPP).

The objectives of this study are to (1) simulate and validate the eco-hydrological model at a small catchment scale with various field and flux measurements, (2) scale up carbon and water processes to a regional scale by integrating spatial information derived from high-resolution satellite data, and (3) evaluate drought effect on MODIS land products with upscaled model results.

Materials and methods

Site description

The Gwangneung Experiment Forest (GEF) is located in the west-central part of the Korean peninsula and represents a typical cool-temperate broadleaved forest zone (Fig. 1). The watershed covers 15.8 km^2 area and elevation ranges from 58 to 619 m. GEF is composed of many vegetation patches of DBF and evergreen needleleaf forest (ENF) characterized by different stand ages and disturbance history. In general, DBF stands are dominated by *Quercus serrata*, *Carpinus laxiflora*, *Q. aliena*, and *Carpinus cordata*, with stand ages ranging from 80 to 200 years and overstory canopy height of 18–20 m (Lim *et al*., 2003). DBF stands are in natural forest without thinning and with an unknown fire history. The average slope of the DBF catchment is about 19.0°, with an area of about 22 ha. ENF stands are dominated by *Pinus koraiensis* and *Pinus banksiana* with a mean canopy height of 16 m. The stands were artificially planted 70–80 years ago and have not experienced thinning with an unknown history of fire. The GEF was registered as the KoFlux network (http://www.koflux.org/) (Kim *et al*., 2006b) and the Korean Long-Term Ecological Research (KLTER) network (Oh *et al*., 2000), respectively. The annual precipitation is 1312.4 mm in 2002, about two-thirds of which falls in a monsoon season from late June to mid-July. The annual mean temperature is 11.3 °C in 2002.

Meteorological data

For this study, we used seven daily meteorological inputs [minimum and maximum temperature, precipitation, average daytime temperature, total shortwave radiation, vapor pressure deficit (VPD) and soil tempera-

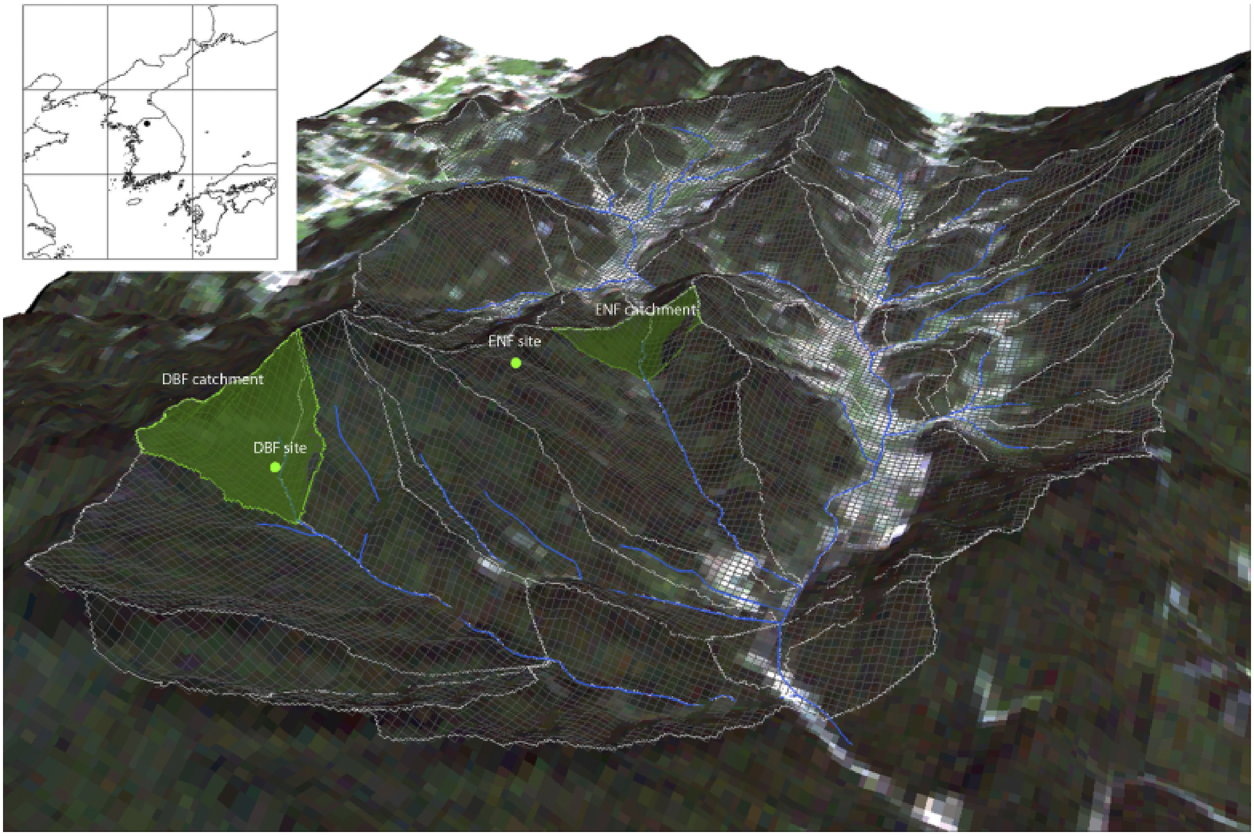

Fig. 1 Hillslope and patch partitioning of the entire watershed. Each patch represents about 30 m × 30 m grid scale, which corresponds to the Landsat ETM+ pixels. ETM+, Enhanced Thematic Mapper plus; ENF, evergreen needleleaf forest; DBF, deciduous broadleaf forest.

ture]. Meteorological data have been measured at the DBF tower site every half hour since September 2001, and aggregated to a daily time step (Fig. 2). From 1997 to 2001, meteorological data from the Gwangneung automatic weather station (Station No. 599) in the study site were used. Before 1997, basic meteorological data (daily minimum and maximum temperature and daily precipitation) were inferred from data of a nearby surface meteorological station in Seoul (Station No. 108) by a simple regression with those from the Gwangneung automatic weathering station.

Field measurements

LAI. LAI, an important determinant in process-based biogeochemical models, is a valuable driver in scaling effort because this value is strongly correlated with normalized difference vegetation index (NDVI) derived from remote sensing images (Gholz *et al.*, 1991; Nemani *et al.*, 1993; Chen & Cihlar, 1996; Fassnacht *et al.*, 1997). Across a broad range of ecosystems, seasonal maximum LAI tends to be correlated with aboveground NPP (Gower *et al.*, 2001; Asner *et al.*, 2003). LAI values were measured at five points randomly around the DBF flux tower and ENF site with a LI-COR 2000 Plant Canopy Analyzer (LI-COR Inc., Lincoln, NE, USA) during 2002. Winter measurements of DBF stands, considered stem area index, were used to correct the measured LAI, while those of ENF were estimated from Chen & Cihlar (1996). The projected LAI for ENF was recalculated by multiplying with a correction factor (needle-to-shoot area ratio) recommended in the literature (Gower & Norman, 1991; Chen & Cihlar, 1996; Gower *et al.*, 1999) to consider the silhouette effect of evergreen needleleaf. The spatial LAI values within the study site were measured at points positioned by a GPS system from July to August 2003 ($n = 32$), regarded as maximum LAI values throughout the year (Fig. 3). The LAI values were compared with Landsat ETM+ NDVI values to derive a map of maximum LAI (Fig. 4a). Each LAI value represents the average of four replicate measurements of LAI values at points of a $30\,m^2$ with a 90° view cap.

 Global Change Biology, doi: 10.1111/j.1365-2486.2008.01556.x

NPP. The annual NPP of 2003 was estimated from biomass increment and foliage production. Total biomass increments were estimated from diameter at breast height (DBH) by tree biometric equations that were developed for dominant woody species within the study site (Lim, 1998). One hundred ten core samples were collected from ten 20 m × 20 m plots around the DBF flux tower, which differ in species composition and slope. Foliage production was measured from the litter traps within the study area in 2003 (Suh *et al.*, 2005). The estimated biomass increment in 2003 was 293.7 $\mathrm{gC\,m^{-2}\,yr^{-1}}$, and foliage production was 128.4 $\mathrm{g\,C\,m^{-2}yr^{-1}}$. If we assume a constant allocation ratio between new fine root and new leaf carbon (1.2 for DBF; White *et al.*, 2000), annual estimated NPP values are 576.2 $\mathrm{g\,C\,m^{-2}\,yr^{-1}}$.

Model parameters. Most major model input parameters were measured on-site (Table 2). Eco-physiological parameters such as C/N ratio, lignin, and specific leaf area, etc. were measured separately both at DBF and ENF stands. Phenological parameters were estimated from a time series of LAI measurements (Fig. 3), observations and MODIS data (Fig. 12). Eleven soil pits were dug around the DBF catchment to measure soil characteristic input parameters (soil texture, porosity, bulk density and rooting depth). These values were used as soil default parameters in the model simulation (Table 2). Leaf turnover ratio of ENF (0.55) was calculated from the ratio of winter LAI to summer LAI values (Fig. 3).

Other field measurements. Other field measurements were conducted intensively at a southeast-facing DBF slope near the flux tower and a northeast-facing ENF slope from September 2001 to July 2003, where elevations are approximately 330/320 m and surface slopes are about 15/23° each. Soil respiration was measured biweekly at five points randomly at both sites using the EGM2 infrared gas analyzer (PP Systems, Hitchin, Hertfordshire, UK). Site-specific temperature scalar functions for both forests (Q_{10} values; Table 2) were also developed for soil respiration using soil temperature data measured simultaneously at 10 cm depth. Volumetric soil water content has been measured every 30 min at five sites around the DBF flux tower at 0–30 cm soil depth with TDR water content reflectometer (Campbell Scientific Inc., Logan, UT, USA). Soil samples were collected from 10 cm depth at both forests biweekly to measure the amount of soil organic carbon in the laboratory. Total soil carbon storage per unit area was calculated from bulk density, percent soil organic carbon and A-horizon depth (Table 2), used to evaluate the initial state of soil carbon storage of the model.

Flux measurements

The flux tower of the DBF stands is located near the outlet of the DBF catchment. Measurements began in September 2001. Fluxes of CO_2, water vapor and sensible heat were measured above the forest by eddy covariance system installed on a 30 m walk-up tower. The system has a fast response infrared gas analyzer (LI7500, LI-COR Inc.) and a three-dimensional sonic anemometer (CSAT3, Campbell Scientific Inc.). Owing to the hilly terrain condition of the study site, the data retrieval rate from the flux tower turned out to be on the order of 10% (Choi *et al.*, 2003). Using this information, daytime NEE was estimated from the relation with photosynthetically active radiation (PAR) measured on-site, and night-time NEE was estimated from soil respiration data. Daily NEE data were recalculated on the basis of these estimated daytime and night-time NEE (Choi *et al.*, 2003).

High-resolution satellite image (Landsat ETM+)

The two Landsat ETM+ images were used for determining spatial pattern of LAI and classifying vegetation types; summer (September 4, 2000) and winter (December 28, 2002). NDVI was calculated with the following equation:

$$\mathrm{NDVI} = \frac{R_{\mathrm{NIR}} - R_{\mathrm{RED}}}{R_{\mathrm{NIR}} + R_{\mathrm{RED}}}, \tag{1}$$

where R_{NIR} is the reflectance within the near-infrared (NIR) and R_{RED} is the reflectance within the red band. NDVI values derived from late summer Landsat ETM+ image before litterfall (September 4, 2000; Fig. 1) were used to calculate the spatial pattern of maximum LAI throughout the year (Fig. 4a). A strong log correlation between measured LAI and calculated NDVI was obtained ($r^2 = 0.86$, $n = 32$; not shown here), which has also been reported by other researchers (Gholz *et al.*, 1991; Nemani *et al.*, 1993; Chen & Cihlar, 1996; Fassnacht *et al.*, 1997). Considering the fact that asymptotic LAI value around saturation is usually about six in the relationship between LAI and NDVI, this method is quite effective within this study area where the maximum LAI is below the saturation point.

The summer and winter images were classified into three land cover classes; DBF, ENF and bare soils. First, the winter image was rectified with summer image, and then bare soil detected from a summer NDVI image was masked. The NDVI image retrieved from a winter image was classified into DBF and ENF. An unsupervised method was used for classifying both images. Urban areas and croplands were stratified into bare soil, while forests were stratified into DBF and ENF (Fig. 4c). Accuracy assessment of land cover classification map

  doi: 10.1111/j.1365-2486.2008.01556.x

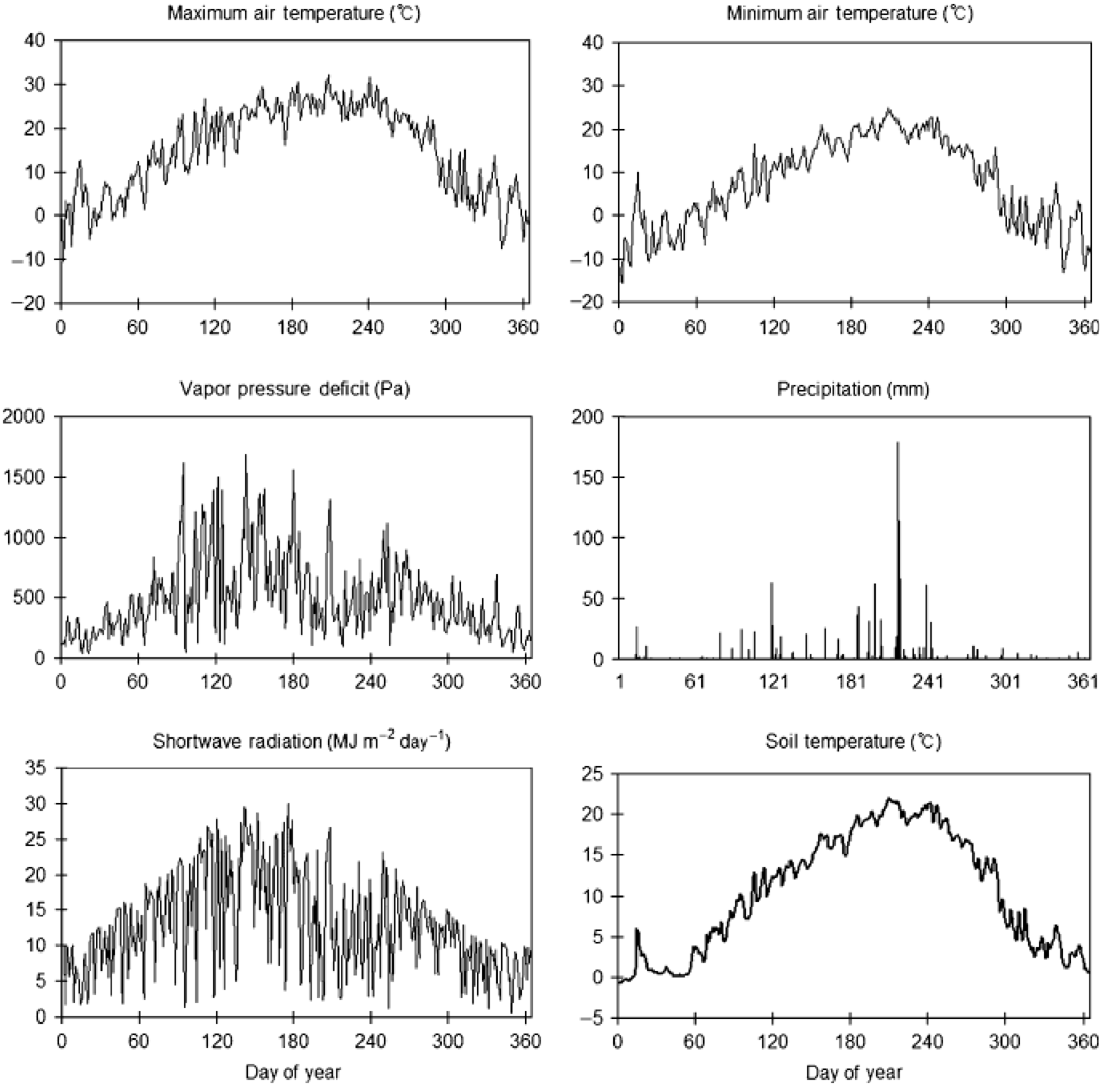

Fig. 2 Yearly meteorological data of DBF flux tower site (2002). DBF, deciduous broadleaf forest.

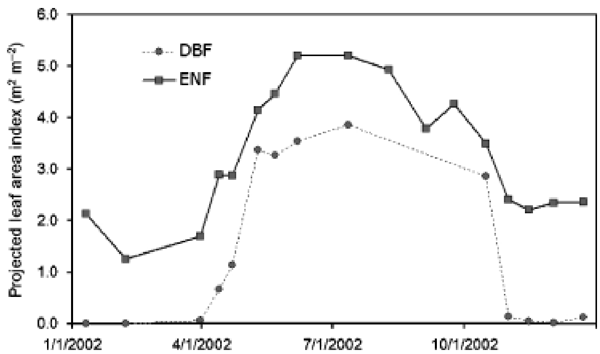

Fig. 3 Seasonal pattern of projected LAI at both biome stands; deciduous broadleaf forest (DBF) and evergreen needleleaf forest (ENF) (each point represents average value of five measurements). LAI, leaf area index.

was carried out pixel by pixel referred with a forest cover map provided by the Korea Forest Research Institute. Overall accuracy is about 62% assuming that each pixel contains only one biome type.

MODIS LAI and GPP/NPP products

The MODIS LAI (MOD15A2) and GPP/NPP (MOD17A2) products were employed to compare with upscaled model results. MOD17 products were reproduced by on-site measured meteorological data from 2001 to 2005 to reduce the error from meteorological data which can be the single largest source of error associated with MODIS GPP/NPP (Zhao *et al.*, 2005; Heinsch *et al.*, 2006). In the production of GPP/NPP

  doi: 10.1111/j.1365-2486.2008.01556.x

estimates, poor quality LAI and fraction of absorbed PAR (FPAR) values were removed based on the quality control (QC) label for each pixel and filled by spatial and temporal linear interpolation (Kang *et al.*, 2005; Zhao *et al.*, 2005). The MODIS land products are produced as the HDF-EOS data format in the Sinusoidal (SIN) projection at the 8-day temporal resolution and an approximately 1 km spatial resolution (Running *et al.*, 2000; Heinsch *et al.*, 2003), reprojected to the GeoTIFF file format with the Universal Transverse Mercator (UTM) coordinate system by MODIS reprojection tool (MRT; http://edcdaac.usgs.gov/landdaac/tools/modis/index.asp). All MODIS data were aggregated to the $5\,\mathrm{km} \times 5\,\mathrm{km}$ grid scale to compare with upscaled model results, large enough to include the entire watershed ($15.8\,\mathrm{km}^2$) and minimize issues of geolocation and representativeness. This aggregated scale was also used for the BigFoot project to evaluate the MODIS GPP product (Turner *et al.*, 2003, 2005).

The MODIS GPP/NPP products strongly depend on MODIS land cover classifications (MOD12Q1; version 3.0) because biome-specific parameters involved in an algorithm are estimated from biome types of MODIS land cover classifications. Within an aggregated $5\,\mathrm{km} \times 5\,\mathrm{km}$ scale, most pixels were classified into mixed forest (MF) with an exception of two pixels of DBF and four pixels of urban area. Therefore, MODIS land cover product within the study area is fairly accurate considering the above land cover composition from the Landsat ETM+ (Fig. 4c), which reduces the possibility of a potential error associated with land cover misclassifications (Heinsch *et al.*, 2006; Zhao *et al.*, 2006).

Model analysis

Process-based eco-hydrological model

RHESSys is a GIS-based, eco-hydrological modeling framework designed to simulate carbon, water and nutrient fluxes (Band *et al.*, 1993; Tague & Band, 2004). RHESSys has been developed from several pre-existing models. First, a microclimate model, MT-CLIM (Running *et al.*, 1987) uses topography and user supplied base station information to extrapolate spatially variable climate variables over topographically varying terrain. Second, an eco-physiological model is adapted from an early version of Biome-BGC (Running & Coughlan, 1988; Running & Hunt, 1993; Kimball *et al.*, 1997) to estimate carbon, water and potential nitrogen fluxes from different canopy cover types. Third, a hydrological model, TOPMODEL (Beven & Kirkby, 1979) is a quasi-distributed model. TOPMODEL distributes soil moisture based on the distribution of a topographically defined wetness index. Fourth, representation of soil organic matter decomposition in RHESSys is largely based on the CENTURY model (Parton *et al.*, 1993). RHESSys also uses the $\mathrm{CENTURY}_{\mathrm{NGAS}}$ (Parton *et al.*, 1996) approach to model nitrogen cycling processes such as nitrification and denitrification. Key processes in RHESSys were shown in Table 1. Detailed explanation of this model is available in the RHESSys homepage (http://fiesta.bren.ucsb.edu/~rhessys/) and Tague & Band (2004).

For this study, recent Biome-BGC (version 4.1.1) changes from the comparison with flux tower data were updated to the current version of RHESSys. These are relevant to the deployment strategy of retranslocated nitrogen and the treatment of daily allocation in the face of a carbon pool deficit (Thornton, 2000).

Model initialization (spin-up process)

A spin-up process in RHESSys simulation is required to allow carbon and nitrogen storages to stabilize, and to build up an organic soil layer. Initial carbon state is quite important in that this value is a major determinant of heterotrophic respiration, which is difficult to estimate as it is so sensitive to long-term disturbance history (Law *et al.*, 2001, 2004). The ranges of soil organic carbon from the spin-up simulation were $11.1 \pm 1.4\,\mathrm{kg\,C\,m^{-2}}$ for DBF and $6.8 \pm 0.8\,\mathrm{kg\,C\,m^{-2}}$ for ENF. These initial states correspond well with on-site measurements throughout the year; $10.8 \pm 2.5\,\mathrm{kg\,C\,m^{-2}}$ for DBF ($n = 135$) and $7.5 \pm 2.0\,\mathrm{kg\,C\,m^{-2}}$ ($n = 250$) for ENF and previous measurements by other researchers; $9.2\,\mathrm{kg\,C\,m^{-2}}$ for DBF ($n = 20$) (Lim *et al.*, 2003).

Model parameterization

Water cycle. Parameterizations were implemented sequentially in water and carbon cycles for the simulation efficiency. The behavioral parameter sets of RHESSys were found first from streamflow prediction, and then LAI. Calibration processes are first conditioned on streamflow data varying m (the decay rate of hydraulic conductivity with depth) and K_{sat0} (saturated hydraulic conductivity at surface) for both lateral and vertical sets with default parameters of carbon cycle. Monte-Carlo simulation was implemented 5000 times with randomly sampled parameter values within certain acceptable ranges. A 3-year calibration period (July 1986 to June 1989) was chosen by considering the representativeness of precipitation patterns and the continuity of streamflow data. At each simulation time, 1.5-year initialization simulation was used before the calibration period to allow soil moisture to stabilize. Nash–Sutcliffe (N–S) coefficient (Nash & Sutcliffe, 1970)

  doi: 10.1111/j.1365-2486.2008.01556.x

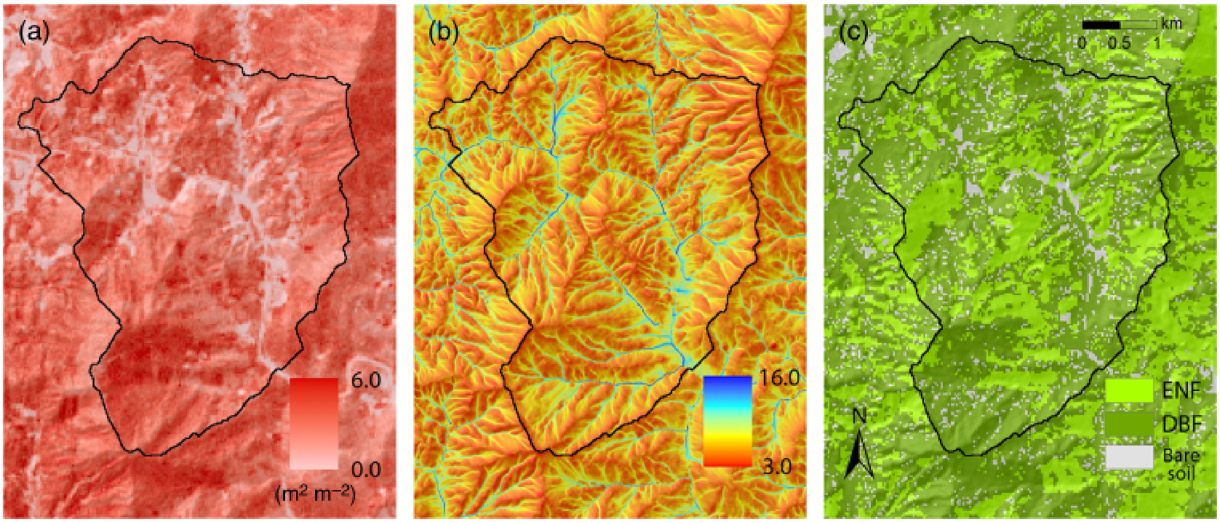

Fig. 4 Spatial pattern of estimated LAI (a), topographic index (b) and vegetation classification (c) in the study site. LAI, leaf area index.

was calculated from the following equation to evaluate model performance:

$$\text{N–S} = 1 - \frac{\sum_{i=1}^{N} (Q_{\text{obs}.i} - Q_{\text{sim}.i})^2}{\sum_{i=1}^{N} (Q_{\text{obs}.i} - \bar{Q}_{\text{obs}})^2}, \quad (2)$$

where $Q_{\text{obs}.i}$ and $Q_{\text{sim}.i}$ is the observed and simulated daily streamflow on ith day and $\bar{Q}_{\text{obs}}$ is the average value for the period being simulated. However, this measure tends to emphasize correspondence between peak flows, which are far higher in this monsoon-dominated climate region. Therefore, log of streamflow values were used in this study to calculate the N–S coefficient as an objective function of calibration.

Carbon cycle. The carbon cycle was calibrated separately at DBF and ENF stands with common optimal water cycle parameters from the DBF catchment under the assumption that hydrological patterns in soils are not significantly affected by biome types within the study area. The *Epc.flnr* (fraction of leaf nitrogen in rubisco) parameter was used to calibrate carbon cycle with LAI data (Fig. 3), known for their high sensitivity (White *et al*., 2000). A trial and error method was employed to minimize the root mean square error (RMSE) between measured and simulated LAI values for both biome types. After this carbon cycle calibration, the N–S coefficient of streamflow simulation was recalculated to check the feedback effect on water cycle by an altered vegetation parameter. The temperature scalar function of heterotrophic respiration was modified to reflect on-site measured Q_{10} values of soil respiration (Table 2). Other eco-physiological and allometric parameters were chosen by following the recommended parameter selections of DBF and ENF biome types in the Biome-BGC model (White *et al*., 2000). All carbon processes were simulated at daily scale at the end of hourly simulations of water processes.

Spatial data assimilation

The RHESSys framework partitions a landscape into a hierarchical spatial structure with levels that are associated with different processes (Tague & Band, 2004). Each level is defined as a particular class type that has specific storage, flux and default variables appropriate for that level. Hillslopes are defined as areas draining into each side of a defined stream link. All other processes were simulated at the same grid scale of the Landsat ETM+ image (i.e. 30 m), allowing modeling of the spatial variance of microclimate, soil water dynamics and vegetation processes at the same scale. This regular grid-based framework is also particularly suitable for application to remote sensing images, where remote sensing image pixels can be treated as the homogeneous spatial units (Chen *et al*., 2005).

A digital elevation model (DEM) in the form of 10 m grid was used to calculate aspect, slope and topographic index map which all are also input raster datasets for RHESSys. Wetness index (or topographic index; Beven & Kirkby, 1979) was calculated by Eqn (3) (Fig. 4b).

$$w_i = \ln\left(\frac{a}{\tan \beta}\right), \quad (3)$$

where w_i is wetness index, a is upslope contributing area per unit contour length and β is local slope. Upslope contributing area was calculated from *D*-infinity ($D\infty$) method, which allows flow to be proportioned between multiple neighboring downslope pixels

Table 1 Key processes of RHESSys model

Processes or parameters	References
Vegetation	
Water	
Interception	f (all-sided LAI)
Transpiration	Penman–Monteith eqn.*
Leaf conductance	f (T, θ, APAR, VPD, CO_2)* (Jarvis, 1976)
Carbon	
Photosynthesis	Farquhar eqn.* (Farquhar *et al*., 1980)
Maintenance respiration	f (T, N, C)* (Ryan, 1991)
Growth respiration	Constant (Biome-BGC)
Allocation/Mortality	Constant (Biome-BGC)
Turnover	Constant (Biome-BGC)
Nitrogen	
Fixed C/N ratio for each compartment	
Retranslocation of stored nitrogen during the litterfall process	
Soil	
Water	
Infiltration	Phillip's eqn.
Drainage	Clapp & Hornberger (1978)
Evaporation/ Capillary rise	Eagleson (1978)
Lateral redistribution	TOPMODEL (Beven & Kirkby, 1979)
Saturated throughflow	TOPMODEL (Beven & Kirkby, 1979)
Carbon	
Heterotrophic respiration	f (T, θ, C, M, N) (Parton *et al*., 1996)
Nitrogen	
Nitrification	f (T, θ, M, NH_4^+) (Parton *et al*., 1996)
Denitrification	f (θ, M, NO_3^-) (Parton *et al*., 1996)
Leaching	Flushing hypothesis
Plant uptake	f (soil mineral N)

*Computed for sunlit and shaded leaves separately.
LAI, leaf area index; T, temperature; θ, rootzone soil moisture contents; APAR, absorbed photosynthetically active radiation; VPD, vapor pressure deficit; N, nitrogen contents; C, substrate (carbon) quality; M, substrate (carbon) storage; RHESSys, Regional Hydro-Ecological Simulation System.

according to gradient (Tarboton, 1997). A prescribed vegetation map classified from Landsat ETM+ image was also used as an input layer (Fig. 4c).

Spatial calibration process

For the application of RHESSys to the entire watershed, the spatial pattern of vegetation derived from Landsat ETM+ image was forced to the model simulation. Even though this study site has not been disturbed much in comparison with other forests in Korea, it is not a perfectly intact region. There are some human land uses such as rice paddy, arboretum, restaurants and inns especially along the stream lines. Therefore, when applying the spatial pattern of vegetation in the model simulation, these patches of different land cover types need to be considered. The stepwise calibration approach cannot consider the human effects on vegetation, most of which were established by artificial gaps within forest. Spatial LAI information cannot be prescribed directly into the model because the model is self-regulating with respect to LAI. The spatial output of maximum LAI in the first run can be regarded as a potential vegetation growth, where microclimate, soil moisture and intraspecific controls are the only constraints for vegetation growth without anthropogenic and other disturbances. Therefore, the ratio of the estimated LAI from the satellite image to potential LAI values was considered as a cover fraction, which means the ratio of vegetation cover within a subpixel. This cover fraction map was reused as input data, by which value all initial state variables were also multiplied.

Results

Validation with streamflow data

A maximum N–S coefficient for the DBF catchment during the 3-year calibration period (July 1986 to June 1989) is 0.78 (Fig. 5b), while that of the 20-year validation period (January 1982 to December 2000) is 0.41 (Fig. 5c). Using the same parameter values, the N–S coefficient of the ENF catchment during the validation period is 0.52 (not shown here), which suggesting the DBF calibration is adequate for representation of soil hydrologic properties in the ENF catchment. Even though there can be a number of possible reasons for the differences between measured and simulated streamflow during the long validation period, the major source of error might be incorrect precipitation data. On-site measured precipitation data were not available during most of the validation period. Instead, regressed precipitation data from the nearby weather station (Seoul; Station No. 108) were used for model simulation. For this reason, several mismatches of rainfall events were found between precipitation and streamflow data.

Validation with field and flux measurements

Modeled soil respiration shows fairly good agreement with measured data for both forest types ($r^2 = 0.92$; Fig. 6a). The simulated annual soil respiration at patch

Table 2 On-site measured eco-physiological parameters and soil characteristics

	Sample number	DBF	ENF
C/N ratio			
Leaf (SD)	5	21.4 (1.46)	29.7 (5.68)
Leaf litter (SD)	5	56.6 (10.1)	58.7 (7.33)
Lignin (%)			
Leaf litter (SD)	3	50.4 (0.28)	50.4 (0.19)
Fine root	1	53.3	51.3
Specific leaf area (SLA, $m^2\,kg^{-1}$)	10	28.5	na
Q_{10} values for soil respiration	150/140	4.37	4.29
Phenology (julian days)			
Leaf on (period)	2	105 (45)	95 (60)
Leaf off (period)	2	280 (40)	275 (90)
Soil properties			
Saturated hydraulic conductivity			
A horizon ($m\,day^{-1}$)	11	32.6 (21.7)	na
B horizon ($m\,day^{-1}$)	11	18.9 (6.0)	na
Texture (%) (sand/clay/silt)	3	62.2/20.3/17.5	na
Porosity (SD)	11	0.49 (0.071)	na
Bulk density (kg soil L^{-1}) (SD)	11	0.877 (0.077)	na
Rooting depth (m) (SD)	11	0.74 (0.18)	na

scales were about $991 \pm 112.4\,g\,C\,m^{-2}\,yr^{-1}$ on 2002, close to the amount of soil respiration estimated from soil temperature and soil water contents at the same site ($1107\,g\,C\,m^{-2}\,yr^{-1}$; Kang *et al*., 2003a). Evaluating soil respiration is quite important as upscaling targets of carbon flux are GPP/NPP units, composed of flux tower NEE estimates and ecosystem respiration terms. Simulated volumetric soil water content fits well with measured data except for the winter season ($r^2 = 0.87$; Fig. 6b). During the winter season, the fluctuations of simulated soil moisture are significantly decreased by an effect of snow cover or freezing effects in the model, not observed in measurement data. However, overall fluxes during the dry winter season are too small to result in a significant bias at a long-term scale.

The seasonal patterns of calculated and simulated daily NEE shows a relatively good correlation ($r^2 = 0.56$; Fig. 7a). Total annual estimated NEE of the deciduous forest is $-232.2\,g\,C\,m^{-2}\,yr^{-1}$ on 2002. This suggests that the deciduous forest in GEF acts as a carbon source, mostly due to very high levels of heterotrophic respiration. Even though fully effective daily evapotranspiration (ET) data were obtained only from 12 days for 1 year (June 2002 to September 2003), it shows a good agreement with simulated daily ET for the deciduous catchment (Fig. 7b).

Total simulated annual NPP for the DBF catchment is $598.5 \pm 23.5\,g\,C\,m^{-2}\,yr^{-1}$ on 2003, while the estimated annual NPP from biometric equation and foliage production is $576.2\,g\,C\,m^{-2}\,yr^{-1}$ (Fig. 8). Annual total ET is $564.5\,mm\,yr^{-1}$ at the DBF catchment in 2002, whereas total ET is $737.1\,mm\,yr^{-1}$ (56.2%) at the ENF catchment. Annual ET can be estimated from the mass balance equation by subtracting annual streamflow from annual precipitation assuming that there is not so much change in soil water storage. These annual ET estimates correspond to the simulated values and follow their interannual variations fairly well (Fig. 8). Spatial patterns of annual NPP and ET within the DBF catchment are also shown in Fig. 9.

Interannual variations of NPP and ET

The long-term model simulation of the DBF catchment clearly shows a severe drought effect on NPP in 2001, also indicated in radial growth measurements (Fig. 8). This severe drought effect on radial growth measurements is unprecedented during the past decade, and is an accumulative effect following the moderate drought in 2000. Interestingly, model results can also simulate the slight NPP overshoot of ring increment data in 1999 and follow those interannual patterns very well.

Figure 9a shows that the spatial pattern of annual NPP estimates during the extreme drought year (2001) is more sensitive to the soil moisture gradients than that of the moderate year (2002). A spatial variation of simulated NPP within the DBF catchment increases during the drought year in spite of their small amounts (Figs 8 and 9a). It strongly suggests that spatial distributions of annual NPP estimates should be more dependent on soil moisture gradient particularly during the drought year. This severe drought effect should

  doi: 10.1111/j.1365-2486.2008.01556.x

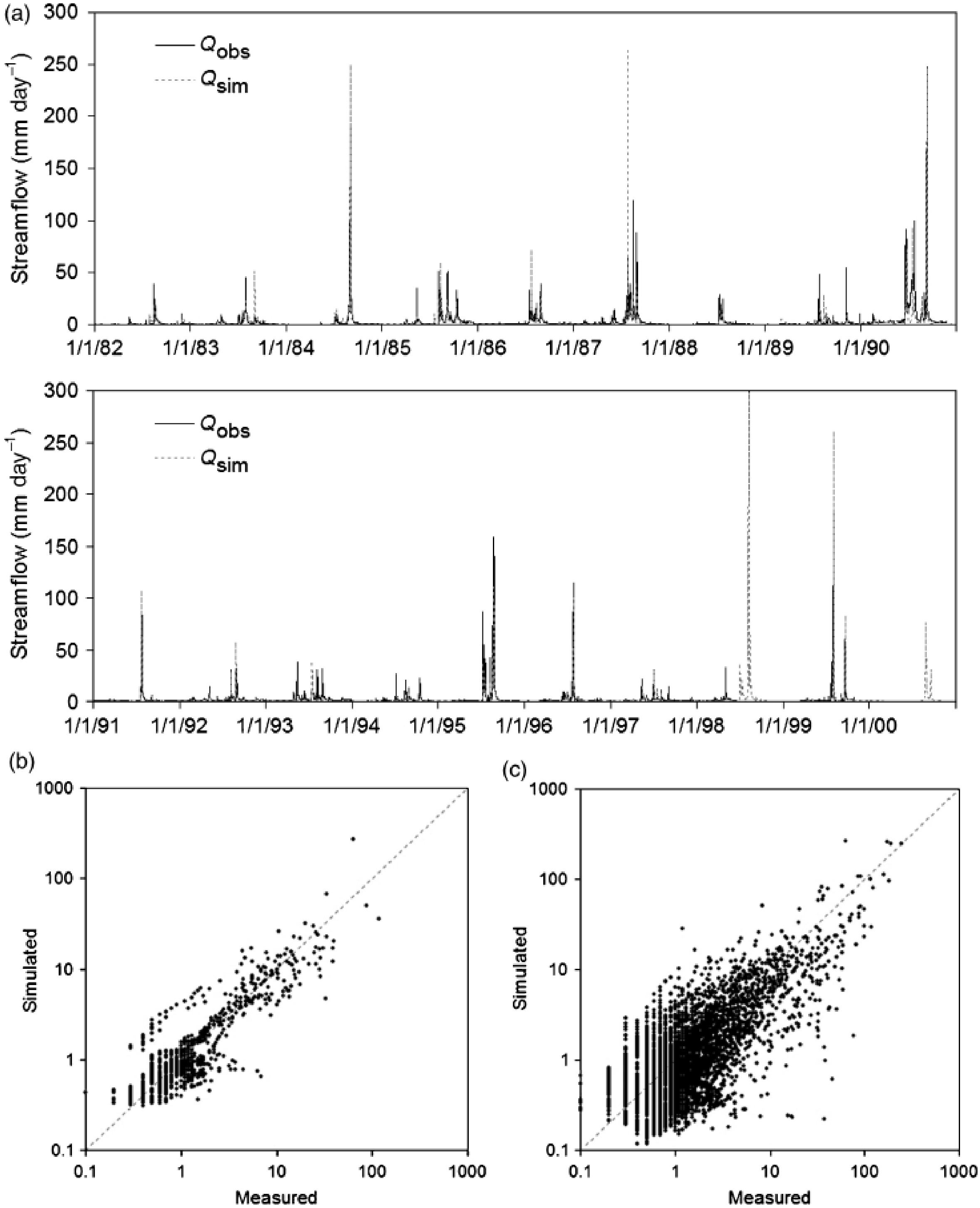

Fig. 5 Observed (Q_{obs}) and simulated (Q_{sim}) streamflow data in the DBF catchment (1982–2000) (a), the log scatter plot of calibration period (b) and validation period (c). DBF, deciduous broadleaf forest.

be mainly dependent on soil water stress rather than VPD or temperature, because the spatial patterns of those two are functions of the elevational gradients in the model.

ET also shows a very similar temporal and spatial drought pattern with NPP (Figs 8 and 9b). Although both NPP and ET clearly show drought effect all over the DBF catchment in 2001 (Fig. 9), carbon uptake (NPP)

  doi: 10.1111/j.1365-2486.2008.01556.x

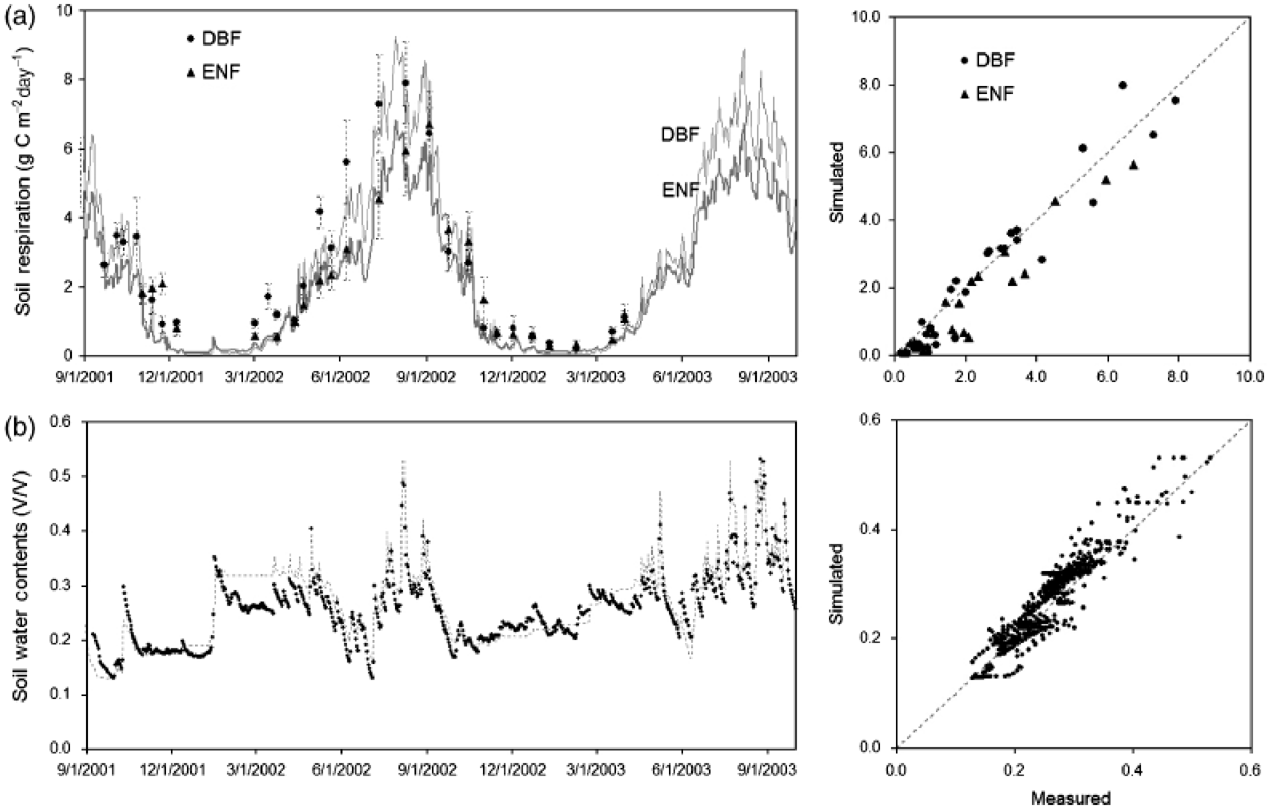

Fig. 6 Seasonal patterns and scatter plots of soil respiration (a) and soil water contents (b) within the DBF catchment (points are measurements and lines are simulation). DBF, deciduous broadleaf forest.

seems to be more sensitive to the drought than water loss (ET). This also indicates a decrease of water use efficiency (WUE) during the drought condition. In the model algorithm, evaporation is more persistent than transpiration in dry conditions, as incoming precipitation first enters interception storage and may not recharge soil moisture. Therefore, evaporation during the drought condition can effectively decouple from carbon uptake.

Model results at the entire watershed

The spatial patterns of NPP and ET show a composite effect of vegetation cover, microclimate and topography. Some examples of model simulation for shortwave downward radiation, daily average temperature, rootzone soil moisture and water table depth are shown (Fig. 10). Direct shortwave radiation maps show clear topographic effects between different slopes, while daily average temperature is mainly affected by elevation information. Water table depth is more fully connected within a hillslope following the TOPMODEL assumption, whereas rootzone soil water content, which is more affected by local water balance by vegetation within a rootzone layer especially during the dry period.

Total annual NPP within the entire watershed ranges from $337.4 \pm 103.4\,\mathrm{g\,C\,m^{-2}\,yr^{-1}}$ (2001) and $504.8 \pm 167.3\,\mathrm{g\,C\,m^{-2}\,yr^{-1}}$ (2002) (Fig. 11a), whereas total annual ET ranges from $435.8 \pm 118.5\,\mathrm{mm\,yr^{-1}}$ (2001) and $512.2 \pm 143.2\,\mathrm{mm\,yr^{-1}}$ (2002) (Fig. 11b). The DBF forest is usually characterized by relatively higher NPP and lower ET values compared with ENF.

Comparison with temporal MODIS data

Consistent overestimation of MODIS LAI during the summer season were observed in this study (Fig. 12a), which were also reported for the Collection 4 MODIS LAI products at other forested sites (Cohen *et al*., 2003, 2006; Fang & Liang, 2005; Leuning *et al*., 2005; Heinsch *et al*., 2006). One possible explanation is understory canopy which was not considered for site measurements and modeling processes (Heinsch *et al*., 2006). However, MODIS LAI values were retrieved from reflectance information for a vertically and horizontally integrated canopy. It seems that the overestimation of the MODIS LAI did not directly result in the

  doi: 10.1111/j.1365-2486.2008.01556.x

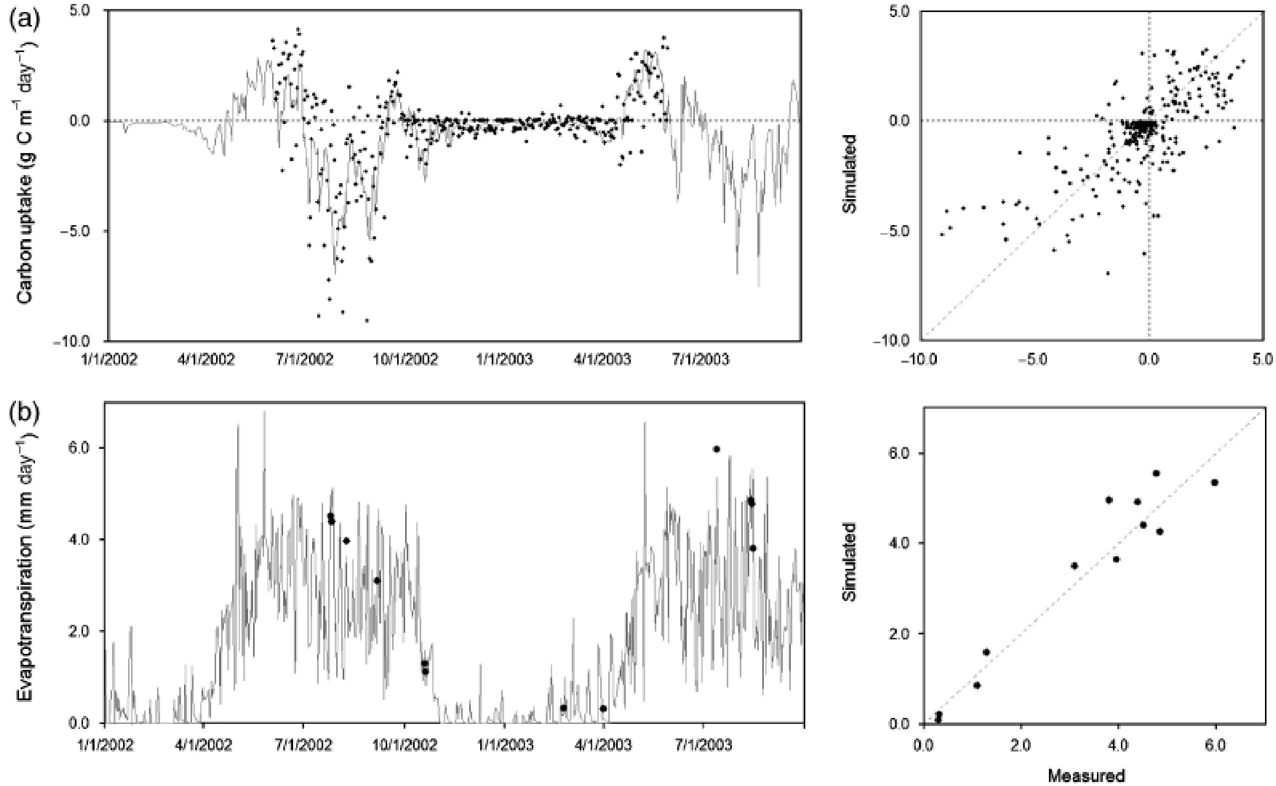

Fig. 7 Seasonal patterns and scatter plots of net ecosystem exchange (NEE) (negative values are carbon sources) (a) and evapotranspiration (ET) (b) within the DBF catchment (points are measurements and lines are simulation). DBF, deciduous broadleaf forest.

overestimation of the MODIS GPP (Fig. 12b). It is mainly because the MOD17 algorithm integrates FPAR values for the radiation use efficiency equation which are not very much different between the ranges of simulated LAI and MODIS LAI with the nonlinear relationship between FPAR and LAI (Myneni *et al.*, 2002). If the LAI overestimation is mostly from the suppressed understory canopy, its contribution to GPP and ET is not that much because of its limited light availability.

A seasonal pattern of simulated GPP shows clear effects by two severe drought events during the early June and the late September in 2001, when we can find considerable overestimation of the MODIS GPP (Fig. 12b). Usually, the spring leaf-on of the MODIS LAI tends to run several weeks earlier than simulated trajectory of LAI, whereas the fall leaf-off of the MODIS LAI tends to be late a week or more. The current version of RHESSys does not incorporate the phenology model to account for environmental controls on the timing of leaf-on and off (White *et al.*, 1997). However, phenological parameters were directly observed on-site for 2002–2003 (Table 2), which means there can be some bias in the MODIS LAI trajectory. Although Kang *et al.* (2003b) reported acceptable representations of phenological seasonality by the MODIS LAI product in the same temperate mixed forest, this kind of bias was observed during the whole simulation period and also reported by other researchers (Fensholt *et al.*, 2004; Turner *et al.*, 2006; Yang *et al.*, 2006). Turner *et al.* (2006) related this bias to leafing out of vernal herbs and understory trees which would be detected by the MODIS sensor but not by site measurements, because the understory may flush out earlier in the season. The MF within this study site is particularly represented by the combination of overstory ENF and understory DBF.

Discussion and conclusions

In this study, an eco-hydrological model, RHESSys, was validated against flux and various field measurements at a catchment scale, and then applied for the simulation of spatial variations of GPP/NPP in a topographically complex forest at the regional scale. The model was calibrated deliberately at a small catchment scale with streamflow and seasonal LAI data for water and carbon cycles sequentially, and then model predictions were validated with a set of separate field measurements (soil water content, soil respiration and NPP/ET estimates) and flux data (NEE, ET). The

  doi: 10.1111/j.1365-2486.2008.01556.x

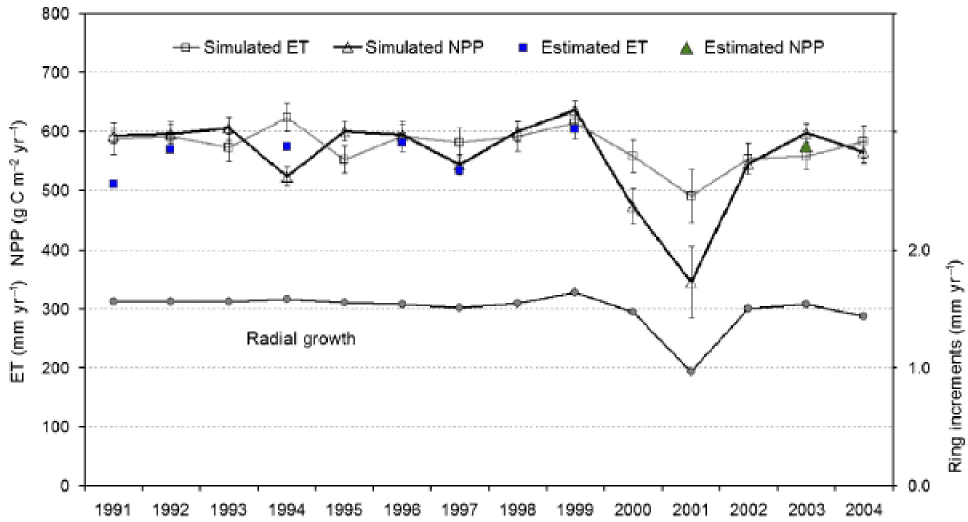

Fig. 8 Interannual variation of simulated annual net primary productivity (NPP; simulated NPP), simulated annual evapotranspiration (ET; simulated ET), annual ET estimated from the water mass balance (estimated ET), annual NPP estimated from biomass increment and foliage production (estimated NPP), and radial growth measurements (radial growth); error bars of NPP and ET represent standard deviations of spatial distribution within the DBF catchment. DBF, deciduous broadleaf forest.

comparison between interannual variations of NPP estimates from the model and ring increment data clearly shows the extreme drought effect in 2001. Water and carbon fluxes were scaled up to evaluate temporal MODIS LAI and GPP products by incorporating spatial information from high-resolution satellite images.

The current MOD17 algorithm integrates two simple linear ramp functions of daily minimum temperature and VPD to produce radiation use efficiency modified from the Monteith equation (Zhao *et al*., 2005, 2006; Heinsch *et al*., 2006), where water stress is only represented by the VPD attenuation function. There are several reasons why water stress is represented by the VPD attenuation function alone in the current MODIS GPP/NPP algorithm (Mu *et al*., 2007). First, it is currently difficult to estimate soil moisture or soil water potential globally at the resolution and domain of the MODIS sensor because of inaccurate global precipitation estimates for driving ecosystem models and tremendous computational load for water mass balance simulation. Second, some studies suggest that atmospheric condition (e.g. VPD) can be an indicator of environmental water stress at a long-term scale (e.g. Nemani *et al*., 2002). Third, MODIS FPAR and LAI estimated from MODIS vegetation indices (NDVI, EVI) partially reflect the water status of the rootzone soil and atmosphere, because water stress can easily result in phenological changes especially in grass-based ecosystems. To date, reliable and consistent estimation of soil moisture from remote sensing platforms have not been developed at the resolution of MODIS.

However, a constraint function of soil water content was typically used at the plot scale in different short-term models for stomatal conductance (Jarvis, 1976; Tardieu & Davies, 1992; Kelliher *et al*., 1995; Oren & Pataki, 2001; Dewar, 2002), because VPD and soil water stress have very different characteristics in terms of spatial and temporal dynamics. Soil moisture has higher spatial variability than VPD due to its strong dependence on topographic gradient and lower temporal variability than VPD due to its buffering effect within a soil column. Therefore, one possible result of this simplification in the MOD17 algorithm is a lack of ability to detect a continuous seasonal drought stress driven by soil water (Turner *et al*., 2005, 2006). Mu *et al*. (2007) have evaluated atmospheric water stress expressed in the MODIS GPP algorithm with full environmental water stress simulated by Biome-BGC over the entire USA and China. They found that atmospheric control cannot capture the seasonality of environmental water stress well in water limited ecosystems in China dominated with a strong summer monsoon cycle than other regions as the summer monsoon easily decouples atmospheric conditions with soil water stress terms. This mismatch between atmospheric controls and soil moisture stress will be particularly significant in mountainous forest areas where soil water patterns are more dependent on topographic drainage.

From long-term model simulation, we found that the interannual variations of simulated NPP estimates were well correlated with radial ring growth patterns. This severe drought effect of NPP was closely related to soil

 Global Change Biology, doi: 10.1111/j.1365-2486.2008.01556.x

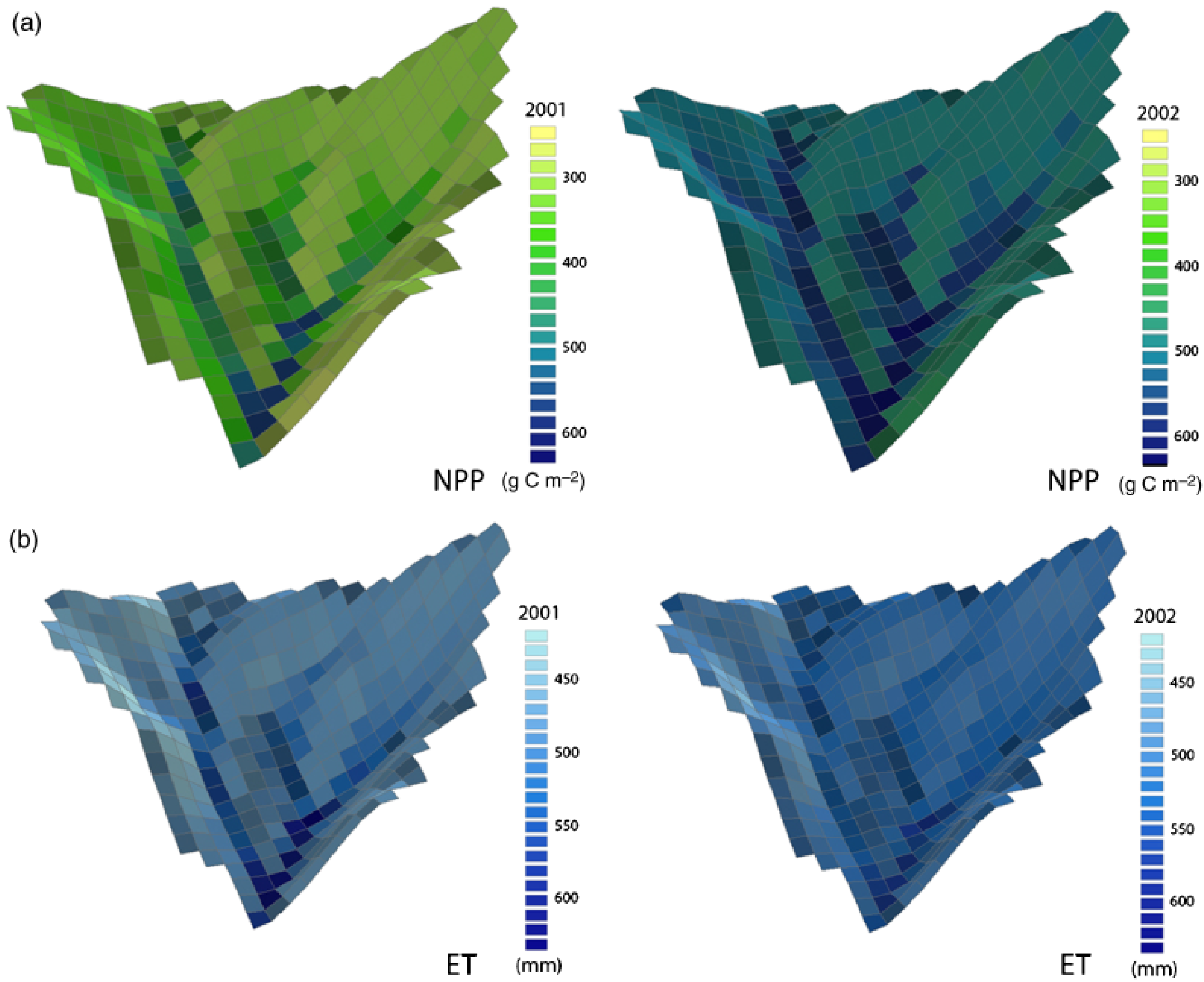

Fig. 9 Spatial patterns of annual net primary productivity (NPP) (a) and annual evapotranspiration (ET) (b) at the DBF catchment in 2001 (extreme drought year) and 2002 (moderate year). DBF, deciduous broadleaf forest.

water stress rather than atmospheric controls (temperature and VPD), and carbon uptake (NPP) seems to be more sensitive to the drought condition than water loss (ET). A recent study in three Mediterranean sites also supports these findings (Reichstein *et al*., 2002). They reported that light-saturated ecosystem gross carbon uptake and daytime averaged canopy conductance declined by up to 90%, closely related to soil water stress. They also found that the observed WUE significantly decreased during the drought events whether ET from eddy covariance or transpiration from sapflow had been used for the calculation. Baldocchi (1997) found a similar result in a deciduous broadleaf forest. In that study, transpiration could be correctly predicted during a moderate drought by decreasing the proportionality constant (the Ball–Berry coefficient) between stomatal conductance and photosynthesis as a function of the cumulative drought index. Leuning *et al*. (2005) also reported important findings by comparing multi-year flux measurements between two contrasting ecosystems in Australia; temperate *Eucalyptus* forest and tropical savanna. They reported that MODIS GPP was significantly overestimated during the dry season (low-rainfall summer), but gave reasonable estimates during the other two wet seasons in a savanna ecosystem where rainfall amount and timing exclusively controls the productivity. In temperate forest, they found that rainfall was a key controlling factor on interannual variations of ecosystem productivity, and ET was less affected by the drought than carbon uptake at the annual scale.

Therefore, the lack of a soil water stress term in the MODIS GPP algorithm may result in significant productivity overestimation particularly during extreme

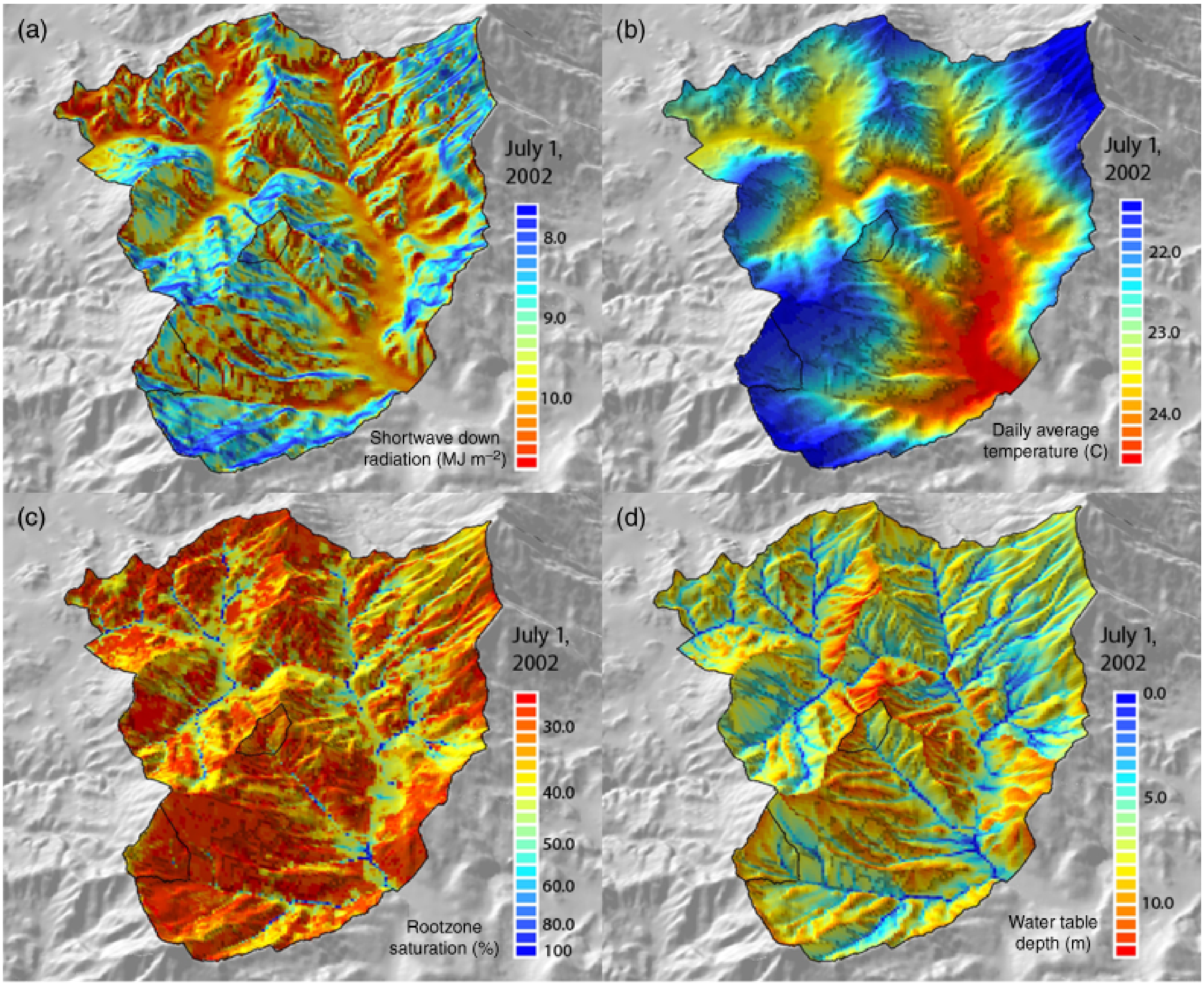

Fig. 10 Spatial patterns of daily shortwave downward radiation (a), daily average temperature (b), rootzone soil water contents (c) and water table depth (d) at the entire watershed on July 1, 2002.

drought. For this reason, there have been recent efforts to estimate soil water potentials from the shortwave infrared and near infrared bands from MODIS and integrate them into the GPP calculation (Xiao *et al*., 2004a, b). Leuning *et al*. (2005) and Pan *et al*. (2006) examined the possible benefits of modifying the MOD17 algorithm by adding a simple water balance scalar from the ratio of antecedent rainfall and potential ET data, and found that it significantly improved the predictions in a savanna ecosystem and a coniferous forest, respectively.

Interannual phenological changes can possibly explain some portion of interannual patterns of carbon uptake in the model (Nemani *et al*., 2002). During the period of this study, about 1-week early leaf-on of MODIS LAI in 2002 and 2003 could explain slightly higher annual MODIS GPP and NPP estimates (Fig. 12b). Interannual variations of carbon uptake by phenological changes cannot be simulated well in this study because the current RHESSys version adopts a constant, prescribed phenology. In spite of this fact, interannual phenological differences in MODIS LAI are not enough to explain the severe drought effect in 2001 clearly shown in ring increment data (Fig. 8). We could not find any phenological anomaly in 2001 by two severe drought events during early June and late September (Fig. 12a). Usually, soil water stress is not a main factor determining phenological changes in trees (White *et al*., 1997). Therefore, drought effect is not effectively captured in tree-based ecosystems with only FPAR and LAI values that represent temporal phenological patterns, whereas drought effects on grass-based

  doi: 10.1111/j.1365-2486.2008.01556.x

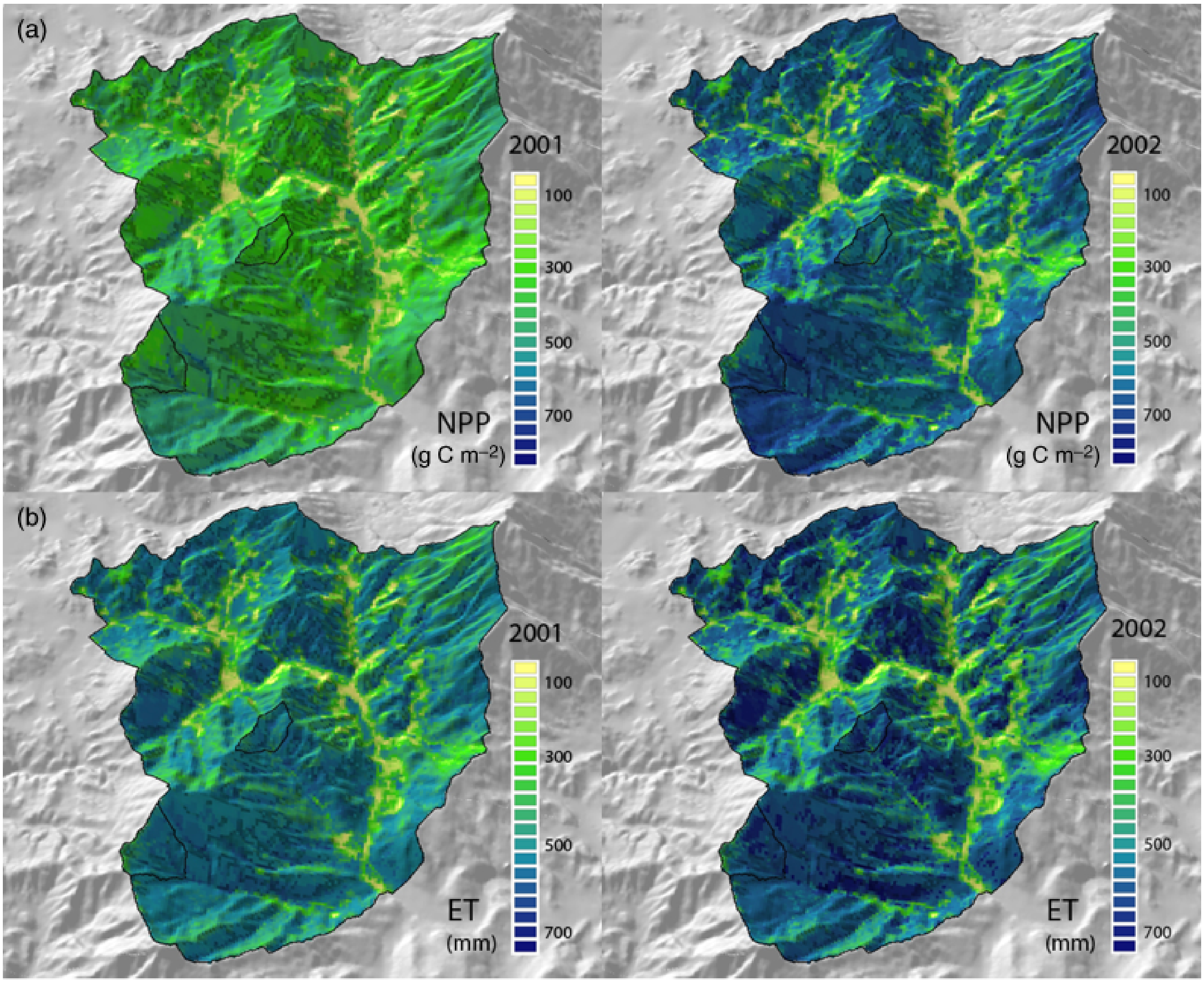

Fig. 11 Spatial patterns of annual net primary productivity (NPP) (a) and annual evapotranspiration (ET) (b) at the entire watershed in 2001 (extreme drought year) and 2002 (moderate year).

(semiarid) ecosystems can be easily detected by their phenological changes (Huete & Didan, 2004; Cheng *et al*., 2006).

We found another potential explanation of productivity overestimation from subspatial and temporal variability at the MODIS scale. Soil moisture variability at footprint scales is usually characterized as increasing positive skewness with decreasing mean soil moisture content, so that positively skewed asymmetric distribution functions (e.g. β, γ) represent spatial variability better, particularly under dry conditions (Famiglietti *et al*., 1998, 1999; Ryu & Famiglietti, 2005). Furthermore, water and carbon processes respond nonlinearly to soil water stress below a certain critical point, whereas the VPD attenuation function in the current MODIS GPP algorithm was represented by its linear ramp effect (Heinsch *et al*., 2003, 2006; Zhao *et al*., 2005). For this reason, simply averaging subgrid variability of environmental water stress may underestimate the effect of severe drought due to the asymmetric nature of the spatial distribution of soil moisture along with its nonlinear effect on water and carbon processes (e.g. Band *et al*., 1993). Especially in mountainous areas, soil moisture can have significant subgrid variability at the MODIS spatial scale, mainly dependent on topographic variability and drainage within a pixel. Moreover, many mountainous forests are more vulnerable to drought because lateral water fluxes through shallow soil columns are dominant within the watershed system. This indicates the potential for overestimation of productivity especially during drought season by simply averaging subgrid variability of soil water contents. It would be useful to further explore the incorporation of subgrid scale variability

  doi: 10.1111/j.1365-2486.2008.01556.x

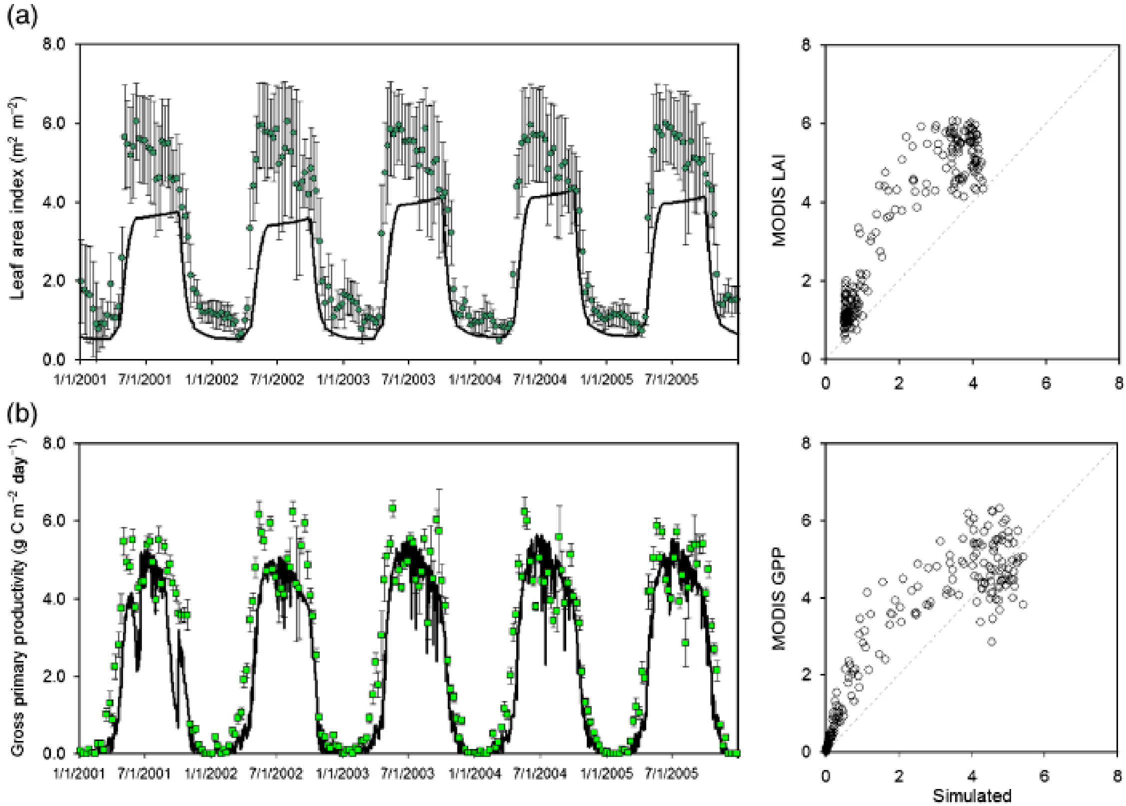

Fig. 12 Temporal evaluation and scatter plots between simulated LAI and MODIS LAI products (a) and simulated GPP and MODIS GPP products (b) at the entire watershed scale (points represent MODIS products and lines represent simulation); error bars of LAI and GPP represent standard deviations of spatial distribution within the 5×5 aggregation unit. LAI, leaf area index; MODIS, Moderate Resolution Imaging Radiometer; GPP, gross primary production.

correction factors to address these issues of bias during drought conditions in important mountainous forest ecosystems.

Aggregated classification and parameterization could also be a potential source of error due to suppression of heterogeneity at the subgrid scale even though the MODIS land cover products are fairly accurate around this study area. The Biome Parameter Look-Up Table (BPLUT) related with MOD17 algorithm (Zhao *et al*., 2005) follows the C3 MODIS land cover classification (MOD12Q1, C3), which simplifies the biome types within an unit pixel. Most of this study area is classified as 'mixed forest,' but about 65% of this study area is classified as DBF. The BPLUT of 'mixed forest' is not weight averaged by subgrid vegetation compositions. Therefore, the wide range of the vegetation composition was treated with a single set of modal biome parameters. Pan *et al*. (2006) suggested that inaccuracy of annual MODIS NPP estimates was possibly related with simple parameterization of radiation use efficiency for diverse deciduous forests from comparing MODIS NPP estimates with forest inventory and analysis (FIA) data. However, this is an intrinsic problem for the global application of the MODIS algorithm (Heinsch *et al*., 2006).

Acknowledgements

This paper was supported by the 'Sustainable Water Resources Research Center of 21st Century Frontier Research Program' (Grant code: 1-8-3), 'Eco-technopia 21' project from the Ministry of Environment, 'BK21 program' from the Ministry of Education and Human Resource Management of Korea, and 'Long-term ecological research under changing global environment' project from the Korea Forest Research Institute. We are very grateful to anonymous reviewers and Dr Conghe Song for valuable comments to improve the manuscript.

References

Aber JD, Reich PB, Goulden ML (1996) Extrapolating leaf CO_2 exchange to the canopy: a generalized model of forest photosynthesis compared with measurements by eddy correlation. *Oecologia*, **V106**, 257–265.

Asner GP, Scurlock JMO, Hicke JA (2003) Global synthesis of leaf area index observations: implications for ecological and remote sensing studies. *Global Ecology and Biogeography*, **12**, 191–205.

Baldocchi D (1997) Measuring and modelling carbon dioxide and water vapour exchange over a temperate broad-leaved forest during the 1995 summer drought. *Plant, Cell and Environment*, **20**, 1108–1122.

Baldocchi D, Falge E, Gu LH *et al*. (2001) FLUXNET: a new tool to study the temporal and spatial variability of ecosystem-scale carbon dioxide, water vapor, and energy flux densities. *Bulletin of the American Meteorological Society*, **82**, 2415–2434.

Band LE, Patterson P, Nemani R, Running SW (1993) Forest ecosystem processes at the watershed scale: incorporating hillslope hydrology. *Agricultural and Forest Meteorology*, **63**, 93–126.

Beven K, Kirkby M (1979) A physically-based variable contributing area model of basin hydrology. *Hydrologic Science Bulletin*, **24**, 43–69.

Chen JM, Chen XY, Ju WM, Geng XY (2005) Distributed hydrological model for mapping evapotranspiration using remote sensing inputs. *Journal of Hydrology*, **305**, 15–39.

Chen JM, Cihlar J (1996) Retrieving leaf area index of boreal conifer forests using landsat TM images. *Remote Sensing of Environment*, **55**, 153–162.

Cheng Y, Gamon JA, Fuentes DA *et al*. (2006) A multi-scale analysis of dynamic optical signals in a Southern California chaparral ecosystem: a comparison of field, AVIRIS and MODIS data. *Remote Sensing of Environment*, **103**, 369–378.

Choi TJ, Kim J, Lim JH (2003) CO_2 exchange in Kwangneung experimental broadleaf deciduous forest in a hilly terrain in the summer of 2002. *Korean Journal of Agricultural and Forest Meteorology*, **5**, 70–80.

Cienciala E, Running SW, Lindroth A, Grelle A, Ryan MG (1998) Analysis of carbon and water fluxes from the NOPEX boreal forest: comparison of measurements with FOREST-BGC simulations. *Journal of Hydrology*, **213**, 62–78.

Clapp RB, Hornberger GM (1978) Empirical equations for some soil hydraulic-properties. *Water Resources Research*, **14**, 601–604.

Cohen WB, Maiersperger TK, Turner DP *et al*. (2006) MODIS land cover and LAI collection 4 product quality across nine sites in the western hemisphere. *IEEE Transactions on Geoscience and Remote Sensing*, **44**, 1843–1857.

Cohen WB, Maiersperger TK, Yang ZQ *et al*. (2003) Comparisons of land cover and LAI estimates derived from ETM plus and MODIS for four sites in North America: a quality assessment of 2000/2001 provisional MODIS products. *Remote Sensing of Environment*, **88**, 233–255.

Dewar RC (2002) The Ball–Berry–Leuning and Tardieu–Davies stomatal models: synthesis and extension within a spatially aggregated picture of guard cell function. *Plant, Cell and Environment*, **25**, 1383–1398.

Eagleson PS (1978) Climate, soil, and vegetation. 3. Simplified model of soil-moisture movement in liquid-phase. *Water Resources Research*, **14**, 722–730.

Falge E, Tenhunen J, Baldocchi D *et al*. (2002) Phase and amplitude of ecosystem carbon release and uptake potentials as derived from FLUXNET measurements. *Agricultural and Forest Meteorology*, **113**, 75–95.

Famiglietti JS, Devereaux JA, Laymon CA *et al*. (1999) Ground-based investigation of soil moisture variability within remote sensing footprints during the Southern Great Plains 1997 (SGP97) hydrology experiment. *Water Resources Research*, **35**, 1839–1851.

Famiglietti JS, Rudnicki JW, Rodell M (1998) Variability in surface moisture content along a hillslope transect: Rattlesnake Hill, Texas. *Journal of Hydrology*, **210**, 259–281.

Famiglietti JS, Wood EF (1994) Application of multiscale water and energy-balance models on a tallgrass prairie. *Water Resources Research*, **30**, 3079–3093.

Fang HL, Liang SL (2005) A hybrid inversion method for mapping leaf area index from MODIS data: experiments and application to broadleaf and needleleaf canopies. *Remote Sensing of Environment*, **94**, 405–424.

Farquhar GD, Caemmerer SV, Berry JA (1980) A biochemical-model of photosynthetic CO_2 assimilation in leaves of C_3 species. *Planta*, **149**, 78–90.

Fassnacht KS, Gower ST, MacKenzie MD, Nordheim EV, Lillesand TM (1997) Estimating the leaf area index of North Central Wisconsin forests using the Landsat Thematic Mapper. *Remote Sensing of Environment*, **61**, 229–245.

Fensholt R, Sandholt I, Rasmussen MS (2004) Evaluation of MODIS LAI, fAPAR and the relation between fAPAR and NDVI in a semi-arid environment using in situ measurements. *Remote Sensing of Environment*, **91**, 490–507.

Gholz HL, Vogel SA, Cropper WP, McKelvey K, Ewel KC, Teskey RO, Curran PJ (1991) Dynamics of canopy structure and light interception in *Pinus elliottii* stands, North Florida. *Ecological Monographs*, **61**, 33–51.

Gower ST, Krankina O, Olson RJ, Apps M, Linder S, Wang C (2001) Net primary production and carbon allocation patterns of boreal forest ecosystems. *Ecological Applications*, **11**, 1395–1411.

Gower ST, Kucharik CJ, Norman JM (1999) Direct and indirect estimation of leaf area index, f(APAR), and net primary production of terrestrial ecosystems. *Remote Sensing of Environment*, **70**, 29–51.

Gower ST, Norman JM (1991) Rapid estimation of leaf area index in conifer and broad-leaf plantations. *Ecology*, **72**, 1896–1900.

Heinsch FA, Reeves M, Votava P *et al*. (2003) *User's Guide, GPP and NPP (MOD17A2/A3) Products*. NASA MODIS Land Algorithm.

Heinsch FA, Zhao MS, Running SW *et al*. (2006) Evaluation of remote sensing based terrestrial productivity from MODIS using regional tower eddy flux network observations. *IEEE Transactions on Geoscience and Remote Sensing*, **44**, 1908–1925.

Huete A, Didan K (2004) MODIS seasonal and inter-annual responses of semiarid ecosystems to drought in the Southwest U.S.A. *Geoscience and Remote Sensing Symposium, 2004. IGARSS '04. Proceedings. 2004 IEEE International*, **3**, 1538–1541.

Jarvis PG (1976) The interpretation of the variations in leaf water potential and stomatal conductance found in canopies in the field. *Philosophical Transactions of the Royal Society of London. Series B, Biological Sciences*, **273**, 593–610.

Kang S, Doh S, Lee D, Lee D, Jin VL, Kimball JS (2003a) Topographic and climatic controls on soil respiration in six temperate mixed-hardwood forest slopes, Korea. *Global Change Biology*, **9**, 1427–1437.

Kang S, Kim S, Lee D (2002) Spatial and temporal patterns of solar radiation based on topography and air temperature. *Canadian Journal of Forest Research*, **32**, 487–497.

Kang S, Lee D, Lee J, Running SW (2006) Topographic and climatic controls on soil environments and net primary production in a rugged temperate hardwood forest in Korea. *Ecological Research*, **21**, 64–74.

Kang S, Running SW, Lim JH, Zhao MS, Park CR, Loehman R (2003b) A regional phenology model for detecting onset of greenness in temperate mixed forests, Korea: an application of MODIS leaf area index. *Remote Sensing of Environment*, **86**, 232–242.

Kang S, Running SW, Zhao M, Kimball JS, Glassy J (2005) Improving continuity of MODIS terrestrial photosynthesis products using an interpolation scheme for cloudy pixels. *International Journal of Remote Sensing*, **26**, 1659–1676.

Kelliher FM, Leuning R, Raupach MR, Schulze ED (1995) Maximum conductances for evaporation from global vegetation types. *Agricultural and Forest Meteorology*, **73**, 1–16.

Kim J, Guo Q, Baldocchi DD, Leclerc M, Xu L, Schmid HP (2006a) Upscaling fluxes from tower to landscape: overlaying flux footprints on high-resolution (IKONOS) images of vegetation cover. *Agricultural and Forest Meteorology*, **136**, 132–146.

Kim J, Lee D, Hong JY *et al*. (2006b) HydroKorea and CarboKorea: cross-scale studies of ecohydrology and biogeochemistry in a heterogeneous and complex forest catchment of Korea. *Ecological Research*, **21**, 881–889.

Kimball JS, Thornton PE, White MA, Running SW (1997) Simulating forest productivity and surface-atmosphere carbon exchange in the BOREAS study region. *Tree Physiology*, **17**, 589–599.

Law BE, Thornton PE, Irvine J, Anthoni PM, Van Tuyl S (2001) Carbon storage and fluxes in ponderosa pine forests at different developmental stages. *Global Change Biology*, **7**, 755–777.

Law BE, Turner D, Campbell J, Sun OJ, Van Tuyl S, Ritts WD, Cohen WB (2004) Disturbance and climate effects on carbon stocks and fluxes across Western Oregon USA. *Global Change Biology*, **10**, 1429–1444.

Leuning R, Cleugh HA, Zegelin SJ, Hughes D (2005) Carbon and water fluxes over a temperate *Eucalyptus* forest and a tropical wet/dry savanna in Australia: measurements and comparison with MODIS remote sensing estimates. *Agricultural and Forest Meteorology*, **129**, 151–173.

Lim JH (1998) *A forest dynamics model based on topographically-induced heterogeneity in solar radiation and soil moisture on the Kwangneung experimental forest*. Unpublished PhD thesis, Seoul National University, Seoul, Korea.

Lim JH, Shin JH, Jin GJ, Chun JH, Oh JS (2003) Forest stand structure, site characteristics and carbon budget of the Kwangneung natural forest in Korea. *Korean Journal of Agricultural and Forest Meteorology*, **5**, 101–109.

Mu QZ, Zhao MS, Heinsch FA, Liu ML, Tian HQ, Running SW (2007) Evaluating water stress controls on primary production in biogeochemical and remote sensing based models. *Journal of Geophysical Research-Biogeosciences*, **112**, G01012.

Myneni RB, Hoffman S, Knyazikhin Y *et al*. (2002) Global products of vegetation leaf area and fraction absorbed PAR from year one of MODIS data. *Remote Sensing of Environment*, **83**, 214–231.

Nash JE, Sutcliffe JV (1970) River flow forecasting through conceptual models part I – a discussion of principles. *Journal of Hydrology*, **10**, 282–290.

Nemani R, Pierce L, Running S, Band L (1993) Forest ecosystem processes at the watershed scale – sensitivity to remotely-sensed leaf area index estimates. *International Journal of Remote Sensing*, **14**, 2519–2534.

Nemani R, White M, Thornton P, Nishida K, Reddy S, Jenkins J, Running S (2002) Recent trends in hydrologic balance have enhanced the terrestrial carbon sink in the United States. *Geophysical Research Letters*, **29**, 1468.

Oh JS, Shin JH, Lim JH (2000) Long-term ecological research programme in Korea Forest Research Institute. *Korean Journal of Ecology*, **23**, 131–134.

Oren R, Pataki DE (2001) Transpiration in response to variation in microclimate and soil moisture in southeastern deciduous forests. *Oecologia*, **127**, 549–559.

Pan Y, Birdsey R, Hom J, McCullough K, Clark K (2006) Improved estimates of net primary productivity from MODIS satellite data at regional and local scales. *Ecological Applications*, **16**, 125–132.

Parton WJ, Mosier AR, Ojima DS, Valentine DW, Schimel DS, Weier K, Kulmala AE (1996) Generalized model for N-2 and N_2O production from nitrification and denitrification. *Global Biogeochemical Cycles*, **10**, 401–412.

Parton WJ, Scurlock JMO, Ojima DS *et al*. (1993) Observations and modeling of biomass and soil organic-matter dynamics for the grassland biome worldwide. *Global Biogeochemical Cycles*, **7**, 785–809.

Reichstein M, Tenhunen JD, Roupsard O *et al*. (2002) Severe drought effects on ecosystem CO_2 and H_2O fluxes at three Mediterranean evergreen sites: revision of current hypotheses? *Global Change Biology*, **8**, 999–1017.

Rodriguez-Iturbe I (2000) Ecohydrology: a hydrologic perspective of climate-soil-vegetation dynamics. *Water Resources Research*, **36**, 3–9.

Running SW, Coughlan JC (1988) A general-model of forest ecosystem processes for regional applications. I. Hydrologic balance, canopy gas-exchange and primary production processes. *Ecological Modelling*, **42**, 125–154.

Running SW, Hunt ER (1993) Generalization of a forest ecosystem process model for other biomes, BIOME-BCG, and an application for global-scale models. In: *Scaling Physiological Processes: Leaf to Globe* (eds Ehleringer JR, Field CB), pp. 141–158. Academic Press Inc., San Diego, CA.

Running SW, Nemani RR, Heinsch FA, Zhao MS, Reeves M, Hashimoto H (2004) A continuous satellite-derived measure of global terrestrial primary production. *Bioscience*, **54**, 547–560.

Running SW, Nemani RR, Hungerford RD (1987) Extrapolation of synoptic meteorological data in mountainous terrain and its use for simulating forest evapotranspiration and photosynthesis. *Canadian Journal of Forest Research*, **17**, 472–483.

Running SW, Thornton PE, Nemani R, Glassy JM (2000) Global terrestrial gross and net primary productivity from the earth observing system. In: *Methods in Ecosystem Science* (eds Sala

  doi: 10.1111/j.1365-2486.2008.01556.x

OE, Jackson RB, Mooney HA, Howarth RW), pp. 44–57. Springer-Verlag, New York.

Ryan MG (1991) Effects of climate change on plant respiration. *Ecological Applications*, **1**, 157–167.

Ryu D, Famiglietti JS (2005) Characterization of footprint-scale surface soil moisture variability using Gaussian and beta distribution functions during the Southern Great Plains 1997 (SGP97) hydrology experiment. *Water Resources Research*, **41**, W12433.

Schimel D, Kittel TGF, Running S, Monson R, Turnispeed A, Anderson D (2002) Carbon sequestration studied in western US mountains. *EOS Transactions*, **83**, 445.

Suh SU, Min YK, Lee JS (2005) Seasonal variation of contribution of leaf-litter decomposition rate in soil respiration in temperate deciduous forest. *Korean Journal of Agricultural and Forest Meteorology*, **7**, 57–65.

Tague CL, Band LE (2004) RHESSys: regional hydro-ecologic simulation system – an object-oriented approach to spatially distributed modeling of carbon, water, and nutrient cycling. *Earth Interactions*, **8**, 1–42.

Tarboton DG (1997) A new method for the determination of flow directions and upslope areas in grid digital elevation models. *Water Resources Research*, **33**, 309–319.

Tardieu F, Davies WJ (1992) Stomatal response to abscisic-acid is a function of current plant water status. *Plant Physiology*, **98**, 540–545.

Thornton PE (2000) *User's Guide for Biome-BGC, Version 4.1.1*. Numerical Terradynamic Simulation Group, University of Montana, Missoula, MT, USA.

Turner DP, Ritts WD, Cohen WB *et al*. (2003) Scaling gross primary production (GPP) over boreal and deciduous forest landscapes in support of MODIS GPP product validation. *Remote Sensing of Environment*, **88**, 256–270.

Turner DP, Ritts WD, Cohen WB *et al*. (2005) Site-level evaluation of satellite-based global terrestrial gross primary production and net primary production monitoring. *Global Change Biology*, **11**, 666–684.

Turner DP, Ritts WD, Cohen WB *et al*. (2006) Evaluation of MODIS NPP and GPP products across multiple biomes. *Remote Sensing of Environment*, **102**, 282–292.

White MA, Thornton PE, Running SW (1997) A continental phenology model for monitoring vegetation responses to interannual climatic variability. *Global Biogeochemical Cycles*, **11**, 217–234.

White MA, Thornton PE, Running SW, Nemani RR (2000) Parameterization and sensitivity analysis of the BIOME-BGC terrestrial ecosystem model: net primary production controls. *Earth Interactions*, **4**, 1–85.

Xiao XM, Hollinger D, Aber J, Goltz M, Davidson EA, Zhang QY, Moore B (2004a) Satellite-based modeling of gross primary production in an evergreen needleleaf forest. *Remote Sensing of Environment*, **89**, 519–534.

Xiao XM, Zhang QY, Braswell B, Urbanski S, Boles S, Wofsy S, Berrien M, Ojima D (2004b) Modeling gross primary production of temperate deciduous broadleaf forest using satellite images and climate data. *Remote Sensing of Environment*, **91**, 256–270.

Yang WZ, Tan B, Huang D *et al*. (2006) MODIS leaf area index products: from validation to algorithm improvement. *IEEE Transactions on Geoscience and Remote Sensing*, **44**, 1885–1898.

Yeakley JA, Swank WT, Swift LW, Hornberger GM, Shugart HH (1998) Soil moisture gradients and controls on a southern Appalachian hillslope from drought through recharge. *Hydrology and Earth System Sciences*, **2**, 41–49.

Zhao M, Heinsch FA, Nemani RR, Running SW (2005) Improvements of the MODIS terrestrial gross and net primary production global data set. *Remote Sensing of Environment*, **95**, 164–176.

Zhao M, Running SW, Nemani RR (2006) Sensitivity of Moderate Resolution Imaging Spectroradiometer (MODIS) terrestrial primary production to the accuracy of meteorological reanalyses. *Journal of Geophysical Research-Biogeosciences*, **111**, G01002.

Zheng DL, Hunt ER, Running SW (1996) Comparison of available soil water capacity estimated from topography and soil series information. *Landscape Ecology*, **11**, 3–14.

  doi: 10.1111/j.1365-2486.2008.01556.x